Modeling the Size-of-Source Effect in Thermography Using a Measured MTF Extended by a Parametric Scattering Model

by Jannik Ebert*, Miguel-David Mendez-Bohorquez*, Robert Schmoll*, Andreas Kroll*

* *Measurement and Control Research Group, University of Kassel, Kassel, Germany*

Abstract

The size-of-source effect (SSE) in thermography describes a systematic deviation of the measured temperature of an object in relation to its size. In this work, the SSE and the modulation transfer function (MTF) were measured for a long-wave infrared (LWIR) camera. The measured MTF was extended by a parametric model to account for low spatial frequency effects, such as scattering, which are not captured by standard measurements. Finally, the SSE was modeled based on the extended MTF, enabling an improved description of the SSE within a linear systems framework and highlighting the dominant role of low spatial frequency contributions, particularly for large objects.

1. Introduction

The size-of-source effect (SSE) is among the largest contributors to measurement uncertainty in thermography, often leading to measurement results that exceed the manufacturer's specified uncertainty range [1, 2]. It describes a systematic deviation of the measured temperature of an object with respect to its size and results from a variety of effects, such as diffraction, signal discretization by the detector, pixel crosstalk, aberrations, and scattering [3, 4, 5].

To quantify this effect, the Association of German Engineers (VDI) has proposed a standard [6] in which circular apertures of different diameters are used to restrict the radiating area of a blackbody heat plate radiator. Here, different aperture sizes represent differently sized measurement objects at constant temperature. In this case, the measured temperature depends on the size of the object, with smaller objects appearing to be colder in the image. Consequently, the SSE can be specified as the relationship between the measured temperature and the diameter of the measured object.

Modeling the SSE is challenging since the underlying effects are inherent to the physical properties of the components of the camera system, such as the optics and the detector. However, Budzier and Gerlach provide a theoretical approach [7], where the SSE is explained by the modulation transfer function (MTF) from linear optics. The MTF causes a reduction of the contrast, particularly for small objects in the image. On this basis, later studies have investigated the quantitative relationship between the MTF and the SSE. In this case, the MTF is used to model [8] and to compensate [2] the SSE. However, it has been found that the MTF fails to fully explain the SSE, especially for large objects in the image.

To overcome this limitation, this study proposes an improved description of the SSE by extending the MTF with a parametric scattering model. The following section is intended to clarify the procedure employed by introducing the fundamentals of the MTF, its relationship with the SSE, and the role of scattering effects. On this theoretical basis, an experimental study of the MTF and the SSE has been conducted for a long-wave infrared (LWIR) camera. The measurement procedure and the SSE modeling approach are illustrated in Section 3. Finally, the evaluation of the results is outlined in Section 4, which compares the (MTF- and scattering-based) modeled SSE to the measured SSE.

2. Fundamentals

This section introduces the fundamentals of the MTF, its relationship with the SSE, and the theoretical basis for the SSE modeling approach presented in this work.

2.1 The Modulation Transfer Function and its Relationship with the Size-of-Source Effect

The MTF describes the spatial frequency response of an optical (linear and shift-invariant) system and is commonly used as a quantitative measure of optical imaging performance [9]. It is defined as the (normalized) magnitude of the optical transfer function (OTF), which itself is the Fourier transform $\mathcal{F}$ of the system's normalized two-dimensional spatial impulse response, commonly referred to as the point spread function (PSF) [3]:

$$MTF(f_\mathrm{x}, f_\mathrm{y}) = \left| \frac{\mathcal{F}\{PSF(x,y)\}}{\mathcal{F}\{PSF(x,y)\}_{f_\mathrm{x}=0,\, f_\mathrm{y}=0}} \right| \tag{1}$$

Here, f_x and f_y denote the spatial frequencies along the corresponding detector coordinates x and y. According to the literature [3, 4, 5, 10], the PSF is the two-dimensional system's response to a point source and arises from the Fraunhofer diffraction pattern, with additional discretization introduced by the detector. While the corresponding MTF is inherently two-dimensional, it is assumed to be rotationally symmetric within a linear system's framework. Consequently, only a one-dimensional profile of the system response is typically evaluated along one of the principal axes of the detector [11].

Optical systems are composed of several components, such as lenses, optical filters, apertures, and a detector. In this case, the overall one-dimensional system MTF is given by the product of the MTFs of all considered subsystems. Two important contributions are the optical MTF, denoted by MTF_{O}, and the detector MTF, denoted by MTF_{D}. These describe the limitations of the system caused by diffraction in the optics and discretization in the detector, respectively [3], in resolving spatial details:

$$MTF_{\mathrm{Sys}}(f_{\mathrm{x}}) = MTF_{\mathrm{O}}(f_{\mathrm{x}}) \cdot MTF_{\mathrm{D}}(f_{\mathrm{x}}) \tag{2}$$

The effects described by the MTF lead to a reduction in image contrast and form the basis for understanding the SSE, where small objects (associated with high spatial frequencies) appear colder in the image. Therefore, the SSE of an optical system can be modeled by convolving artificial input data (ideal images containing objects of varying sizes at a constant temperature) with the PSF, resulting in the degraded system output. Consequently, the decrease in the MTF at high spatial frequencies directly leads to a reduction in contrast for small objects, thereby explaining, within a linear system's framework, the size-dependent response characteristics of the SSE.

2.2 Modulation Transfer Function in the Presence of Scattered Radiation

Besides diffraction and discretization, additional factors, such as pixel crosstalk, aberrations, internal reflections, scattering, and stray light, also contribute to the system's MTF [3, 4, 5] and, consequently, the SSE. In previous work, such contributions have been observed as a sharp decline in the measured MTF at low spatial frequencies [8].

To describe, within a linear systems framework, this effect mathematically, the Harvey–Shack surface scatter theory [12, 13] is employed. When a specular beam of radiation is emitted by a point source and transmitted [14] through a smooth optical surface, part of the radiation is scattered. Therefore, the spatial impulse response of the optical surface consists of two components: A specular beam that remains unaffected by the surface and a minor diffuse component caused by scattering, both represented by the angle spread function (ASF)

$$ASF(\alpha, \beta) = A \cdot \delta(\alpha, \beta) + S(\alpha, \beta) \tag{3}$$

along the coordinates α and β. Here, A is the radiant power fraction of the specular component, given by the Dirac delta function δ. The scattering function S defines the shape of the scattered irradiance distribution. In analogy to the MTF, the projected spatial impulse response of a single smooth optical surface at small incident angles can be expressed by a surface transfer function (STF)

$$STF(f_{\mathrm{x}}) = \mathcal{F}\big\{ASF(\alpha, \beta)\big\} = A + B \cdot ACV(f_{\mathrm{x}}) \tag{4}$$

where $B = 1 - A$ denotes the radiant power fraction of the scattered component and ACV is the autocovariance function of the surface profile, which is usually assumed to follow a Gaussian distribution [13].

Finally, the extended MTF of an optical system in the presence of surface scattering is given by the product of the classical MTF and the STF:

$$MTF_{\mathrm{Ext}}(f_{\mathrm{x}}) = MTF_{\mathrm{Sys}}(f_{\mathrm{x}}) \cdot STF(f_{\mathrm{x}}) \tag{5}$$

The STF introduces a sharp decline in the MTF (see Section 4, Fig. 5), which is consistent with previous MTF measurements [8]. Note that this effect cannot be attributed exclusively to surface scattering. Additional contributions, such as stray light, Rayleigh scattering, and internal reflections, may produce similar effects. Nevertheless, the Harvey–Shack theory provides a convenient framework to approximate the linear contributions of these combined effects in parametric form.

3. Methodology

In this work, a long-wave infrared (LWIR) camera equipped with a wide-angle optical lens was investigated experimentally. The MTF was determined using the slanted edge method based on the visual imaging standard [11], and the SSE was measured in accordance with [15] and [16]. This section focuses on the measurement procedure and the subsequent modeling of the SSE based on the measured MTF, which is extended by a parametric scattering model.

3.1 Experimental Setup

The MTF and SSE were investigated using an Opris PI450 camera, whose technical specifications are summarized in Table 1. The blackbody heat plate radiator IR-150/301, manufactured by Infrared Systems [17], was used as the source of radiation. It provides a radiating surface of $305\,\mathrm{mm} \times 305\,\mathrm{mm}$ with an emissivity of $\varepsilon = 0.96 \pm 0.02$, a spatial non-uniformity of $\pm 0.1\,\%$ of the temperature setpoint within a $254\,\mathrm{mm} \times 254\,\mathrm{mm}$ central surface, and a short-term temporal stability of $\pm 0.1\,^{\circ}\mathrm{C}$. The camera was placed $220\,\mathrm{mm}$ in front of the radiator to cover its full field of view (FOV). To measure the SSE, two iris diaphragms with different sizes, with manual pin levers, were mounted on metal sheets to realize a wide range of target diameters, ranging from $1\,\mathrm{mm}$ to $34\,\mathrm{mm}$ and from $6\,\mathrm{mm}$ to $120\,\mathrm{mm}$. The MTF was measured according to guideline [11], using a metal sheet as a vertical $15\,^{\circ}$ slanted edge instead of a visual test target. The iris diaphragms and the slanted edge were placed $45\,\mathrm{mm}$ in front of the camera. To minimize the influence of reflections, a coating with an emissivity of $\varepsilon \approx 0.91$ at the camera's effective wavelength [18] was applied to the side of the metal sheet facing the camera. The camera's focus was adjusted manually with the slanted edge and the iris diaphragms, while monitoring the local derivative as a quantitative measure of sharpness. The full experimental setup is illustrated in Fig. 1.

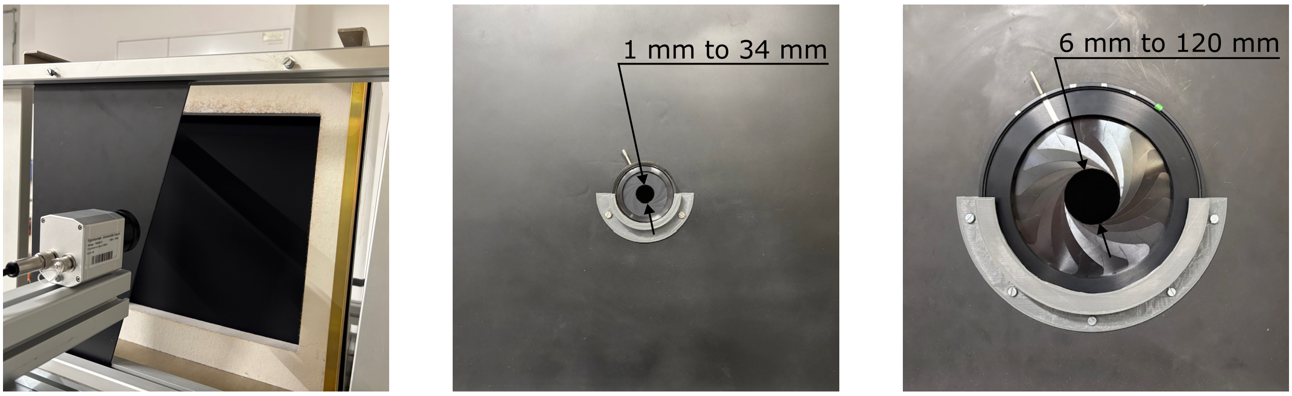

(a) Slanted edge (b) Small iris diaphragm (c) Large iris diaphragm

Fig. 1. *Experimental setup for measuring the MTF with a slanted edge (a) and the SSE with two manually adjustable iris diaphragms (b, c), placed in front of a blackbody heat plate radiator.*

Table 1. *Technical specifications of the investigated LWIR camera Optris PI 450.*

Specification	**Optris PI 450**
Detector	uncooled FPA ($25\,\mu\mathrm{m} \times 25\,\mu\mathrm{m}$)
Image resolution ($w \times h$)	$382 \times 288\,\mathrm{pixels}$
Spectral range	$7.5\,\mu\mathrm{m}$ to $13\,\mu\mathrm{m}$
Temperature ranges	$-20\,^\circ\mathrm{C}$ to $100\,^\circ\mathrm{C}$ $0\,^\circ\mathrm{C}$ to $250\,^\circ\mathrm{C}$ $150\,^\circ\mathrm{C}$ to $900\,^\circ\mathrm{C}$
FOV	$62^\circ \times 49^\circ$
Thermal sensitivity (NETD)	$40\,\mathrm{mK}$
Accuracy	$\pm 2\,^\circ\mathrm{C}$ or $\pm\,2\,\%$ (of measured value)

3.2 Measurement Procedure

The measurements were conducted after the temperature of the radiator had stabilized at the target set point of $200\,^\circ\mathrm{C}$ and the camera was set to a temperature range of $0\,^\circ\mathrm{C}$ to $250\,^\circ\mathrm{C}$. To measure the MTF, the slanted edge was positioned centrally in front of the radiator, and the focus adjusted. To take noise into account, the thermogram of the edge was acquired by averaging a series of 50 frames. Analogously, to measure the SSE, the iris diaphragm was placed in front of the radiator, and the focus adjusted with the iris diaphragm set to its minimum opening size. Immediately thereafter, the SSE was measured by recording a time series while opening and closing the iris diaphragm for two consecutive cycles. To ensure the temperature stability of the radiator, the experiment was conducted within a short time frame of about 10 seconds. After the data was collected, the iris diaphragm was removed, and the camera protected from the heat of the radiator. After two minutes, the temperature stability was verified, and a second dataset acquired, as before. The measurements were repeated for the second iris diaphragm, again following the same procedure, resulting in four separate datasets.

The SSE is evaluated for each dataset by detecting the diameter d of the iris diaphragm in each thermogram using the OpenCV Hough Circle Transform [19, 20], where the largest opening exceeds the camera's FOV, with a maximum detected diameter of $462\,\mathrm{px}$. For each detected diameter, the mean radiance $\overline{L}_{\mathrm{ROI}}(d)$ is measured within a circular region of interest (ROI) with a diameter of 5 pixels in the center of the diaphragm. Finally, the SSE is expressed as

$$SSE(d) := \frac{\overline{L}_{\mathrm{ROI}}(d) - L_{\mathrm{bg}}}{L_{\mathrm{ref}} - L_{\mathrm{bg}}} \tag{6}$$

with a reference radiance L_{ref} and background radiance L_{bg}. In the context of this work, the SSE is described by the system's finite spatial impulse response. Consequently, the SSE is expected to converge when measuring large objects. Therefore, the reference radiance L_{ref} is defined as the radiance of an infinitely large object and is evaluated within the SSE modeling process. In addition, the inclusion of L_{bg} provides a normalization with respect to the background radiance emitted by the diaphragm surface, ensuring that the SSE is independent of the absolute temperature and is bounded between 0 and 1.

3.3 Evaluation of the Modulation Transfer Function

The MTF is evaluated according to guideline [11]: First, a region of interest (ROI) of size $64\,\mathrm{px} \times 140\,\mathrm{px}$ (height $\times$ width) is defined centered around the slanted edge. The 15° angle between the vertical detector axis and the edge allows four adjacent pixel rows to be combined into a single one-dimensional supersampled step response (since $4 \approx \frac{1}{\tan(15°)}$). This procedure is applied successively to all pixel rows within the ROI, and the resulting supersampled edge spread functions (ESFs) are averaged to obtain the final ESF used for the MTF evaluation. The spatial derivative (central difference quotient) of the ESF yields the line spread function (LSF), which serves as a one-dimensional approximation of the well known PSF. Finally, the MTF is obtained by using the discrete Fourier transform of the normalized LSF.

Previous work has demonstrated that, in contrast to visual imaging systems, in which the LSF is typically assumed to be a sharp peak, the selection of the ROI can significantly affect the measured MTF of a thermography camera [8]. In this case, the LSF still appears as a sharp peak but is also characterized by diffuse wings (see Fig 2). Although these wings are often difficult to distinguish from the amplified noise, they significantly contribute to the low spatial frequencies of the MTF and must therefore be taken into account. However, their reliable measurement is challenging, particularly for systems with wide-angle lenses, as the radiator's edge (see Fig. 1) may introduce disturbances that lead to a decay of the ESF toward the boundary of a large ROI, thereby affecting the shape of the wings of the LSF.

Consequently, in the measured LSF, the wings are cut off to isolate the contributions of high spatial frequencies, such as diffraction and discretization. In a subsequent step (see Section 3.4), the wings are modeled to take into account the contributions of low spatial frequencies, including scattering and stray light. To ensure a reproducible cropping of the LSF, a sufficiently wide ROI is preselected around the slanted edge, and the full width at half maximum (FWHM) of the LSF is determined by identifying its peak value and the exact positions at which the signal drops to half of this maximum, using linear interpolation. Finally, a symmetric section around the peak is defined with a width of 12 times the FWHM, rounded to the nearest integer. The selected width is found empirically to provide a robust compromise between the suppression of low spatial frequencies and the preservation of the sharp peak. The obtained LSF is illustrated in Fig. 2.

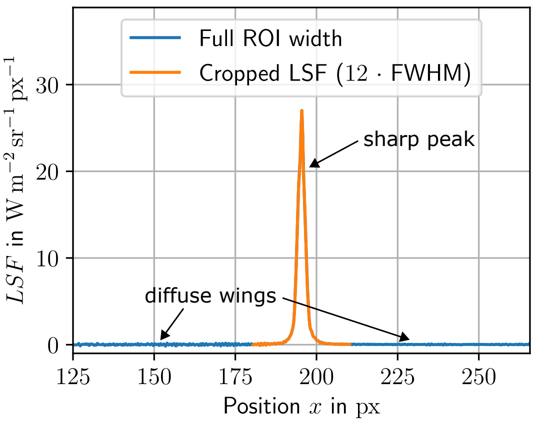

(a) LSF

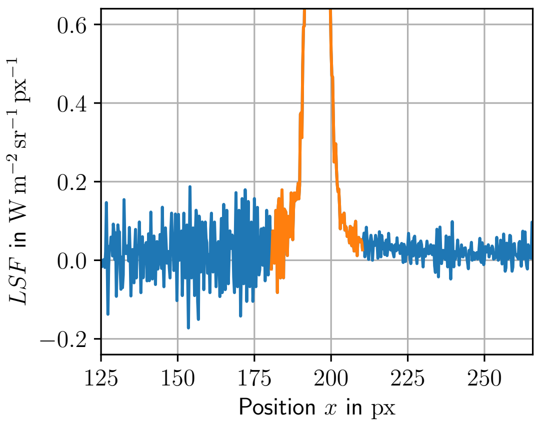

(b) Zoomed in LSF (wings noticeably obscured by noise)

Fig. 2. *Resulting calculated LSF: The LSF (a) is cropped to a width of 12 times the FWHM (= 32 pixel) to isolate the contributions of high spatial frequencies. The outer regions of the LSF, which cannot be reliably evaluated due to amplified noise (b) and the radiator's edge, are cut off and modeled in a subsequent step. The measured MTF MTF_{Meas} is presented in Section 4 (see Fig. 5).*

3.4 Modeling the Size-of-Source Effect

As a result of the LSF cropping discussed in Section 3.3, the measured MTF does not fully capture the contributions of the low spatial frequencies which are necessary to describe the SSE effectively. To take into account these contributions, the modeled MTF

$$MTF_{\mathrm{Model}}(f_{\mathrm{x}}) = MTF_{\mathrm{Meas}}(f_{\mathrm{x}}) \cdot STF_{\mathrm{Param}}(f_{\mathrm{x}}) \tag{7}$$

is defined as the product of the measured MTF MTF_{Meas} and a parametric “scattering“ transfer function

$$STF_{\mathrm{Param}}(f_{\mathrm{x}}) = A + B \cdot \exp\left(-\pi(C \cdot f_{\mathrm{x}})^2\right) \tag{8}$$

with

$$A = 1 - B \tag{9}$$

and the model parameters B and C. The STF, therefore, aims to approximate the missing contributions of the spatial frequencies of the measured MTF and is strongly motivated by the Harvey–Shack surface scatter theory, in which the STF is referred to as the surface transfer function. The shape of the STF (see Section 4, Fig. 5) is based on the assumption that a small fraction B of the radiation is scattered along its path to the detector, resulting in a Gaussian scattering pattern whose width is proportional to the parameter C.

In order to model the SSE, the camera is considered as a black box receiving ideal rectangular input signals

$$I_d(x) = \begin{cases} L_{\mathrm{ref}} & \text{if } |x - \frac{w}{2}| \leq \frac{d}{2} \\ L_{\mathrm{bg}} & \text{if } |x - \frac{w}{2}| > \frac{d}{2} \end{cases} \tag{10}$$

where d denotes the width of the rectangle, x the horizontal detector coordinate, and w the detector width. Each signal represents a one dimensional slice of a circular object with diameter d at constant radiance L_{ref} and background radiance L_{bg}, where L_{ref} is introduced as an additional model parameter and L_{bg} is assumed to correspond to a constant temperature of $20\,^{\circ}\mathrm{C}$, which is equivalent to a radiance of $45.97\,\mathrm{W\,m^{-2}\,sr^{-1}}$. The ideal input signals are convolved with the inverse Fourier transform $\mathcal{F}^{-1}$ of the modeled MTF, producing the modeled output signals

$$O_d(x) = I_d(x) * \mathcal{F}^{-1}\{MTF_{\mathrm{Model}}\} \tag{11}$$

in which the modeled SSE is evaluated for a given set of target diameters. In this case, the convolution is performed as a multiplication in the spatial frequency domain. A schematic overview of the employed modeling approach is given in Fig. 3.

The model parameters L_{ref}, B, and C are estimated by minimizing the mean squared error (MSE) between the modeled and the measured SSE. Due to noise in the measured SSE and the numerical evaluation of the model, a derivative-free optimization approach is employed. The parameter estimation is carried out using the SciPy library with default optimization settings. First, differential evolution [21] is used to obtain a robust initial estimate of parameters B and C while keeping the parameter L_{ref} fixed at the measured radiance of the largest object, $372.78\,\mathrm{W\,m^{-2}\,sr^{-1}}$. Subsequently, all three parameters are jointly refined using the Nelder–Mead algorithm [22, 23], where L_{ref} is no longer fixed. The uncertainty of the parameters is assessed using a bootstrap approach, where the measured SSE is resampled with replacement from the original dataset and the parameter estimation is repeated 20 times. Finally, the mean values and standard deviations of the resulting parameter distributions are derived.

4. Results and Discussion

The estimated model parameters and the RMSE obtained from the bootstrap analysis are summarized in Table 2. Note that the RMSE refers to the absolute values of the radiance of the SSE. Here, Fig. 4 compares the modeled and the measured SSEs. In addition, the modeled SSE is evaluated separately using the measured MTF and the parametric STF to assess the contribution of each component.

The results show that the measured MTF alone is insufficient to fully describe the SSE, although it captures the rapid decline for small diameters of an object. For objects with diameters larger than $100\,\mathrm{px}$, however, the predicted radiance exhibits only minor changes. By extending the measured MTF with the parametric STF, an accurate quantitative description of the SSE is finally achieved.

Fig. 5 presents a comparison between the measured MTF, the parametric STF, and the resulting modeled MTF. In this case, the measured MTF and the modeled MTF both converge toward a common diffraction limit at high spatial frequencies. However, the STF introduces a sharp decline in the modeled MTF at low spatial frequencies, consistent with previous findings [8]. The resulting SSE model reveals that this modeled degradation is a significant contributor to the system’s response and that it is therefore necessary to consider it in the context of the SSE.

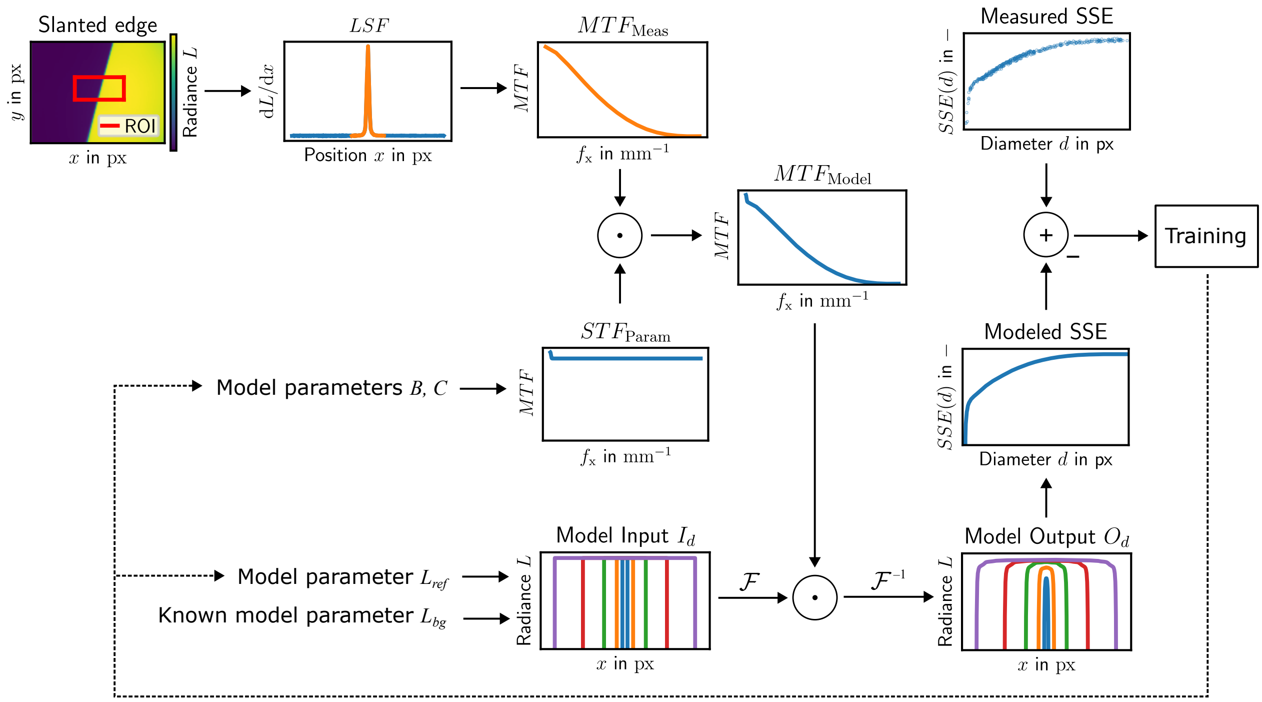

Fig. 3. *SSE modeling approach: The (diffraction-limited) measured MTF is obtained using the slanted-edge method [11]. Multiplication with the (scattering-based) parametric STF yields the modeled MTF. Finally, ideal input signals are multiplied by the modeled MTF in the spatial frequency domain to generate the model output, from which the modeled SSE is evaluated (analogously to Section 3.2). Furthermore, the model parameters are optimized based on the measured SSE.*

5. Conclusion and Outlook

In this work, the SSE of an LWIR camera was investigated experimentally by measuring the SSE and the MTF. To account for low spatial frequency effects that are not captured by standard MTF measurements, the measured MTF was extended by a parametric scattering model based on the Harvey–Shack surface scatter theory. The resulting model was then used to describe, within a linear systems framework, the SSE.

The results demonstrate that the proposed model significantly improves the characterization of the behavior of the system in terms of the SSE. For measuring large objects, diffraction and discretization effects are negligible, whereas low spatial frequency contributions (attributed to scattering and related effects) are more dominant. These findings enhance the understanding of the SSE and suggest that the model can serve as a foundation for correcting the SSE using parametric compensation approaches [2, 24, 25], with parameters informed by physical knowledge. To achieve this, the presented model may be extended to a fully two-dimensional model in future work.

In addition, the comparison of the measured MTF and the modeled MTF reveals that evaluating the MTF in a small ROI may be sufficient for capturing the diffraction limit of the system, but fails to fully describe the behavior of the system, particularly at low spatial frequencies. Since a reliable evaluation of the MTF over a larger ROI is often challenging, the proposed model provides a useful approach to refine measured MTFs by incorporating low spatial frequency effects that are typically neglected in standard measurement procedures.

Table 2. *Estimated model parameters and RMSE (based on absolute values of the radiance) obtained via bootstrap analysis based on 20 realizations with mean μ and standard deviation σ.*

Parameter	Unit	μ	σ
B	–	7.08×10^{-2}	6.57×10^{-4}
C	–	1.73×10^{-1}	1.92×10^{-3}
L_{ref}	$\mathrm{W\,m^{-2}\,sr^{-1}}$	373.53	6.91×10^{-2}
RMSE	$\mathrm{W\,m^{-2}\,sr^{-1}}$	3.62×10^{-1}	3.36×10^{-2}

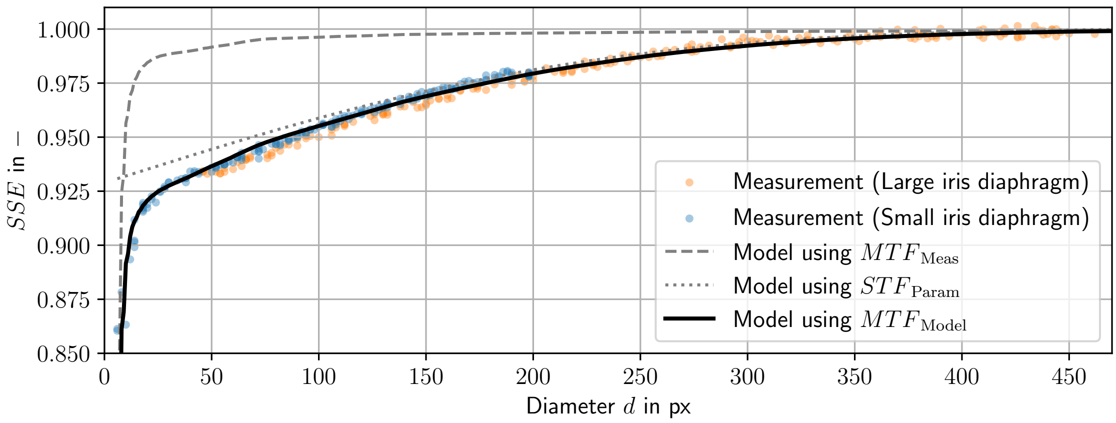

Fig. 4. *Comparison between the measured SSE (using two iris diaphragms of different sizes) and the modeled SSE. The contributions of the measured MTF and the parametric STF to the combined model are illustrated in gray.*

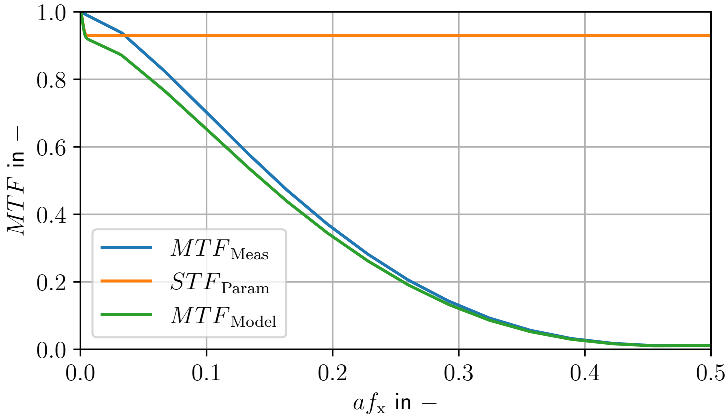

(a) MTF

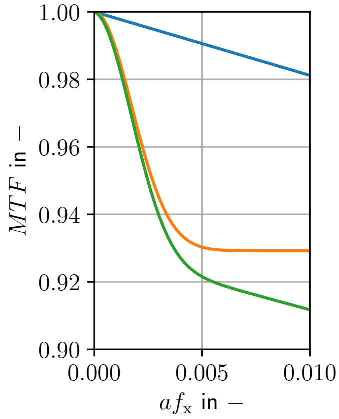

(b) MTF (low spatial frequencies)

Fig. 5. *Comparison between the measured MTF, the parametric STF and the combined modeled MTF over the normalized spatial frequency with pixel pitch $a = 25\,\mu\mathrm{m}$ and the Nyquist frequency at $af_{\mathrm{x}} = 0.5$. The STF introduces a sharp decline in the MTF at low spatial frequencies (b), which improves the description of the SSE by the modeled MTF.*

References

[1] Igor Pušnik and Gregor Geršak. Evaluation of the size-of-source effect in thermal imaging cameras. *Sensors*, 21(2), 2021.

[2] Sebastian Schramm, Jannik Ebert, Robert Schmoll, and Andreas Kroll. Compensating the size-of-source effect: Relationship between the MTF and a data-driven convolution filter approach. In *16th Quantitative InfraRed Thermography Conference (QIRT)*, Paris, France, 2022.

[3] Helmut Budzier and Gerald Gerlach. *Thermal Infrared Sensors: Theory, Optimisation and Practice*. Wiley, 2011.

[4] Glenn D. Boreman. *Modulation Transfer Function in Optical and Electro-Optical Systems, Second Edition*. SPIE, Bellingham, Washington, USA, 2021.

[5] Arnulf Wallrabe, Maurus Tacke, and Reinhard Ebert. *Infrared Cameras: Fundamentals, Technologies, and Systems (in german)*. Springer Vieweg, Wiesbaden, Germany, 2nd edition, 2022.

[6] Verein Deutscher Ingenieure, Germany. *VDI/VDE 5585 Part 1. Temperature Measurement with Thermographic Cameras - Metrological Characterization*, 2018.

[7] Helmut Budzier and Gerald Gerlach. The size-of-source effect in thermography. *Journal of Sensors and Sensor Systems*, 10:179–184, Jul. 2021.

[8] Jannik Ebert, Miguel Mendez, Robert Schmoll, and Andreas Kroll. Assessing the size-of-source effect in thermography by measuring the MTF with consideration of scattering effects. In *2025 IEEE International Instrumentation and Measurement Technology Conference (I2MTC)*, Chemnitz, Germany, May 2025. IEEE Instrumentation and Measurement Society.

[9] ISO 9334:2012: Optics and photonics – optical transfer function – definitions and mathematical relationships, 2012.

[10] Eugene Hecht. *Optics Global Edition*. Pearson Deutschland, 2016.

[11] BS ISO 12233:2017: Photography. Electronic still picture imaging. Resolution and spatial frequency responses, 2017.

[12] James Harvey. Light-scattering characteristics of optical surfaces. *Proceedings of SPIE - The International Society for Optical Engineering*, 107, Jul. 1976.

[13] James Harvey. Parametric analysis of the effect of scattered light upon the modulation transfer function. *Proc SPIE*, 8841:88410W, Sep. 2013.

[14] James Harvey, Narak Choi, and Andrey Krywonos. Scattering from moderately rough interfaces between two arbitrary media. *Proceedings of SPIE - The International Society for Optical Engineering*, 7794:77940V, Aug. 2010.

[15] Miguel-David Mendez-Bohorquez, Jannik Ebert, Lars Sommerlade, Robert Schmoll, and Andreas Kroll. The size of source effect for middle- and long-wavelength infrared cameras: assessment by direct measurements and a modulation transfer function approach. pages 1–18. Taylor & Francis, 2025.

[16] Miguel-David Mendez-Bohorquez, Robert Schmoll, and Andreas Kroll. Rapid measurement of the size-of-source effect by using an iris aperture. In *Sensor and Measurement Science International Conference (SMSI) 2025*, pages 196–197, Nuremberg, Germany, May 2025. AMA Verband für Sensorik und Messtechnik e.V.

[17] Infrared Systems Development Corporation. IR-150/301 Blackbody System, 2026. [Accessed: 2026 Jun. 12].

[18] Lab IR Paints. Thermographic paint for low temperature applications. https://paints.labir.cz/en/paints/herp-lt/. [Accessed: 2026 Jun. 12].

[19] Richard O. Duda and Peter E. Hart. Use of the Hough transformation to detect lines and curves in pictures. *Commun. ACM*, 15(1):11–15, January 1972.

[20] OpenCV.org. Opencv: Open source computer vision library. https://opencv.org/, 2024. Version 4.5.

[21] Rainer Storn and Kenneth Price. Differential evolution – a simple and efficient heuristic for global optimization over continuous spaces. *Journal of Global Optimization*, 11(4):341–359, 1997.

[22] J. A. Nelder and R. Mead. A simplex method for function minimization. *The Computer Journal*, 7(4):308–313, 1965.

[23] Fuchang Gao and Lixing Han. Implementing the Nelder–Mead simplex algorithm with adaptive parameters. *Computational Optimization and Applications*, 51:259–277, May 2012.

[24] Sebastian Schramm, Robert Schmoll, and Andreas Kroll. Compensation of the size-of-source effect of infrared cameras using image processing methods. In *13th International Conference on Sensing Technology (ICST)*, pages 1–6, Sydney, Australia, 2019.

[25] Erik Bryan Beall. Correction of the size-of-source effect in thermal imaging and application to body thermometry. *Sensors*, 26(7):2177, 2026.